The Optimal Control Methods for the Covid-19 Pandemic Model's Precise and Practical SIQR Mathematical Model

R. Ramesh, G. Arul Joseph

Abstract—**The study employs sensitivity analysis and optimal control algorithms to understand the dynamics of COVID-19 comprehensively. It assesses the stability of equilibrium points and computes the basic reproduction number using a next-generation matrix. Additionally, it investigates both the global and local stability of the disease-free equilibrium point and identifies the potential emergence of an endemic equilibrium if the basic reproduction number surpasses one. Sensitivity analysis of the fundamental parameters is conducted, and the model is calibrated with actual COVID-19 case data from India.**

Furthermore, the study extends the model to include optimal control utilizing the Pontryagin maximum principle. This optimal control strategy integrates the use of face masks, hand sanitizers, and isolation as control measures. Mathematical simulations are employed to evaluate the effectiveness and cost-efficiency of various control strategies. Based on the analysis and simulations, the study suggests that the most effective and economically feasible approach to curbing the spread of COVID-19 involves a combination of wearing face masks, using hand sanitizers, and practicing social isolation. This research provides valuable insights into the dynamics of COVID-19, emphasizing the significance of adopting control measures such as wearing face masks, using hand sanitizers, and adhering to social distancing to mitigate the virus's spread.

Index Terms—**SIQR Model, reproduction number, stability analysis, equilibrium.**

I. Introduction

IN December 2019, Wuhan, China, witnessed the emergence of a novel coronavirus strain, swiftly spreading globally and prompting the WHO to declare a pandemic in March 2020. Named COVID-19, this coronavirus is believed to have originated from transmission between snakes and bats to humans, with the initial outbreak traced back to the Wuhan seafood market, as determined by the WHO.

The zoonotic nature of COVID-19 underscores the importance of understanding infectious diseases originating in animals and their potential impact on human health. Additionally, the unprecedented global spread of the pandemic underscores the interconnectedness of our world and the imperative for collaborative efforts in addressing such health crises. International research and collaboration have played a crucial role in combating the virus, showcasing the significance of global cooperation in tackling emerging diseases.

The response to the COVID-19 pandemic highlights the interconnectedness of nations and the essential role of collaboration in addressing and mitigating health crises. Through international cooperation and dedicated research, countries have developed comprehensive strategies to control the spread of COVID-19 and identify effective treatments. These collective efforts emphasize the importance of a unified global response to emerging infectious diseases, highlighting the ongoing need for collaboration and knowledge sharing to safeguard global public health.

The pandemic has not only underscored the necessity of a globally coordinated approach but also emphasized collective responsibility. It has highlighted the importance of nations working together, pooling resources and expertise to confront emerging infectious diseases effectively. The significance of shared knowledge has become increasingly apparent, emphasizing the need for a united front to protect individuals globally.

In essence, the COVID-19 pandemic has emphasized the need for a global response to emerging infectious diseases, underscoring the interconnectedness of nations and the crucial role of international collaboration in addressing health crises. The exemplary global response to the pandemic showcases the importance of fostering international collaboration and maintaining a coordinated approach to combating emerging infectious diseases. Beyond its impact on global health, COVID-19 has disrupted financial markets, educational systems, and social fabric worldwide.

Symptoms of COVID-19 range from coughing, sniffling, and difficulty breathing to fatigue, headache, diminished taste and smell, diarrhea, throat discomfort, and muscular discomfort. Additionally, COVID-19 can affect various bodily functions, including those of the lungs, liver, and kidneys. The mortality rate varies among countries, influenced by environmental factors, dietary habits, and demographic factors such as age and pre-existing conditions like diabetes, cancer, and obesity. Individuals aged 60 and above, especially those with underlying health conditions, face an increased risk of severe infection.

The incubation period of COVID-19 ranges from 2 to 14 days, during which an infected individual may not display symptoms but can transmit the virus to others. Understanding these aspects of the disease is crucial for implementing effective preventive measures and healthcare strategies to mitigate its impact.

Public health professionals and regulators continuously monitor the dynamics and transmission patterns of in-

Manuscript received September 25, 2023; revised June 26, 2024.

R. Ramesh is an Assistant Professor in the Department of Mathematics at Faculty of Engineering and Technology, SRM Institute of Science and Technology, Ramapuram-600 089, Chennai, Tamil Nadu, INDIA. (e-mail: rameshmaths106637@gmail.com).

G. Arul Joseph is an Assistant Professor in the Department of Mathematics at College of Engineering and Technology, Faculty of Engineering and Technology, SRM Institute of Science and Technology, Kattankulathur-603 203, Chengalpattu District, Tamil Nadu, INDIA. (corresponding author e-mail: aruljosg@srmist.edu.in).

fectious diseases to formulate effective control measures. Community-wide education, self-protection initiatives, proper use of face masks, avoiding large gatherings, maintaining physical distance, and regular handwashing are fundamental preventive measures.

Implementing well-designed shutdown strategies and promptly isolating exposed or infected individuals are essential for curbing virus transmission. Vaccination programs targeting high-risk individuals are crucial for building immunity. Collaboration between public health professionals, regulatory bodies, and the general population is instrumental in implementing and sustaining effective control measures.

In the realm of mathematical modeling, researchers strive to devise accurate representations of the virus and formulate control methods to prevent its spread. Our research introduced the SIQR model, categorizing infected individuals into super-spreaders and those in isolation to enhance disease assessment and prevention. This model integrates non-pharmaceutical interventions such as quarantine, health education, and maintaining physical distance to mitigate virus transmission.

In conclusion, the COVID-19 pandemic has highlighted the importance of a global response to emerging infectious diseases and emphasized international collaboration in addressing health crises. The exemplary global response has showcased the significance of fostering collaboration and maintaining a coordinated approach to combating emerging infectious diseases.

II. SIQR MATHEMATICAL MODELING OF INDIAN PANDEMIC COVID-19 EQUATION

Based on the current situation, we categorize the human population into four compartments:

S(t): Individuals susceptible to the virus, Q(t): Those infected and isolated/quarantined, I(t): Individuals showing symptoms of the illness, R(t): Individuals who have recovered from COVID-19. In the Q(t) category, we assume that some infected individuals are placed in quarantine, including those who are isolated as part of this group.

TABLE I: PARAMETER MEANINGS FOR MODEL

Parameters	Description
Λ	Recruitment Rate
β	Disease Transmission Rate from S to I
θ	Disease Transmission Rate from I to Q
α	Recovery Rate from I to R
λ	Recovery Rate from Q to R
γ	Natural Death Rate

$$\begin{aligned}
\tfrac{dS}{dt} &= \Lambda - \beta SI - \gamma S \\
\tfrac{dI}{dt} &= \beta SI - (\gamma + \theta + \alpha)I \\
\tfrac{dQ}{dt} &= \theta I - (\lambda + \gamma)Q \\
\tfrac{dR}{dt} &= \alpha I + \lambda Q - \gamma R
\end{aligned} \tag{1}$$

III. THE INDIAN PANDEMIC COVID-19 EQUATION HAS A BOUNDED SOLUTION

The system's (1) boundedness property.
Let M = S + I + Q + R then

$$\frac{dM}{dt} = \frac{dS}{dt} + \frac{dE}{dt} + \frac{dI}{dt} + \frac{dR}{dt}$$
$$\frac{dM}{dt} = \Lambda - \gamma M$$

then

$$\frac{dM}{dt} + \gamma M \leq \Lambda$$

We may get by integrating the above inequality and applying Birkhoff and Rota's theorem for differential equations.

$$M \leq \frac{\Lambda}{\gamma}[1 - e^{-\gamma t}] + M_0 e^{-\gamma t} \tag{2}$$
$$\text{now for } \boldsymbol{t} \to \infty$$

Hence all the solutions of System of Nonlinear Equations (1) that are commence in R_+^5 are restricted in the region

IV. THE COVID-19 EQUATION'S THE INITIAL ILLNESS TRANSMISSION RATE FOR THE INDIAN PANDEMIC

The initial rate of illness transmission, commonly denoted as R_0, is a numerical measure that impacts the velocity of illness propagation. An epidemic transitions into a pandemic solely when R_0 surpasses 1. This pivotal value is ascertained through the next-generation matrix approach, which involves computing the spectral radius of a square matrix. This spectral radius signifies the maximum absolute value of the eigenvalues of FV^{-1}, where F denotes the Jacobian of infection rate during the recruitment process, and V^{-1} represents the Jacobian of other transmission parameters in disease equations. Therefore, it is appropriate to reference the system as delineated in [18].

$$\begin{aligned}
\tfrac{dI}{dt} &= \beta SI - (\gamma + \theta + \alpha)I \\
\tfrac{dQ}{dt} &= \theta I - (\lambda + \gamma)Q
\end{aligned} \tag{3}$$

We can write the above system as

$$\frac{dy}{dt} = F(y) - V(y)$$
$$y = \begin{pmatrix} I \\ Q \end{pmatrix}, F(y) = \begin{pmatrix} \beta SI \\ 0 \end{pmatrix}, V(y) = \begin{pmatrix} (\gamma + \theta + \alpha)I \\ (\lambda + \gamma)Q - \theta I \end{pmatrix}$$

The absolute maximum eigenvalue of the matrix is used to get the initial disease transmission number $E_0\left(\frac{\Lambda M}{\gamma}, 0, 0, 0\right)$ in the disease-free equilibrium, the Jacobian matrices of F and V are now given by the

$$F = J\left(\tfrac{F}{I_0}\right) = \begin{pmatrix} \beta S^0 & 0 \\ 0 & 0 \end{pmatrix}$$
$$V = J\left(\tfrac{V}{I_0}\right) = \begin{pmatrix} \gamma + \theta + \alpha & 0 \\ -\theta & \lambda + \gamma \end{pmatrix}$$

Then

$$V^{-1} = \frac{1}{(\gamma + \theta + \alpha)(\lambda + \gamma)} \begin{pmatrix} \lambda + \gamma & 0 \\ \theta & \gamma + \theta + \alpha \end{pmatrix}$$

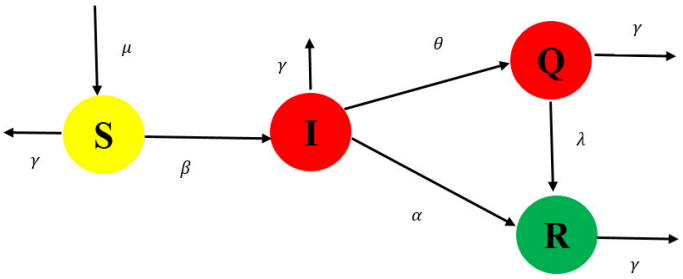

Fig. 1: Under this Assumption the Mathematical Model of Indian Pandemic COVID-19

$$V^{-1} = \begin{pmatrix} \frac{1}{(\gamma+\theta+\alpha)} & 0 \\ \frac{\theta}{(\gamma+\theta+\alpha)(\lambda+\gamma)} & \frac{1}{(\lambda+\gamma)} \end{pmatrix}$$

The initial illness transmission number (R_0) of the matrix FV^{-1} is given by,

$$FV^{-1} = \begin{pmatrix} \beta S^0 & 0 \\ 0 & 0 \end{pmatrix} \begin{pmatrix} \frac{1}{(\gamma+\theta+\alpha)} & 0 \\ \frac{\theta}{(\gamma+\theta+\alpha)(\lambda+\gamma)} & \frac{1}{(\lambda+\gamma)} \end{pmatrix}$$

$$FV^{-1} = \frac{\beta S^0}{(\gamma+\theta+\alpha)}$$

$$R_0 = \frac{\beta\Lambda}{(\gamma)(\gamma+\theta+\alpha)} \tag{4}$$

V. Procedure COVID-19 Equation Equillibrium Solution for INDIA

There are two conceivable equilibrium states within the system. The first is the disease-free equilibrium point, labeled as E_0, where infection is entirely absent from the population and is determined by the initial susceptible population S_0. The second equilibrium point is the endemic equilibrium, denoted as E_1 (S^*, I^*, Q^*, R^*), where infection remains consistently present in the system. This state is characterized by stable values of the susceptible (S^*), infected (I^*), quarantined (Q^*), and recovered (R^*) populations.

$$\begin{aligned} S^* &= \tfrac{\gamma+\theta+\alpha}{\beta} \\ I^* &= \tfrac{\Lambda\beta-\gamma(\gamma+\theta+\alpha)}{\beta(\gamma+\theta+\alpha)} \\ Q^* &= \tfrac{\theta}{\lambda+\gamma}\left(\tfrac{\Lambda\beta-\gamma(\gamma+\theta+\alpha)}{\beta(\gamma+\theta+\alpha)}\right) \\ R^* &= \tfrac{\alpha(\lambda+\gamma)+\theta\lambda}{\gamma(\lambda+\gamma)}\left(\tfrac{\Lambda\beta-\gamma(\gamma+\theta+\alpha)}{\beta(\gamma+\theta+\alpha)}\right) \end{aligned} \tag{5}$$

VI. COVID-19 Indian Pandemic Is Locally Asymptotically Stable

In this part, we examine the regional asymptotic stabilization requirement for various solutions. The disease-free equilibrium, denoted as E_0, is unstable if $R_0 > 1$, but locally asymptotically stable if $R_0 = 1$.The Jacobian matrix of system (1) at a disease-free equilibrium is given by [22].

$$J = \begin{bmatrix} -\gamma & -\beta S_0 & 0 & 0 \\ 0 & \beta S_0 - (\gamma+\theta+\alpha) & 0 & 0 \\ 0 & \theta & -(\gamma+\lambda) & 0 \\ 0 & 0 & 0 & -\gamma \end{bmatrix}$$

$| J - KI |=$

$$\begin{bmatrix} -\gamma-k & -\beta S_0 & 0 & 0 \\ 0 & (\beta S_0 - (\gamma+\theta+\alpha)) - k & 0 & 0 \\ 0 & \theta & -(\gamma+\lambda)-k & 0 \\ 0 & 0 & 0 & -\gamma-k \end{bmatrix}$$

the free of illness stability of characteristic Equn:(1) is now indicated by

$$(k+\gamma)^2(k+\lambda+\gamma)(k+\theta+\gamma+\alpha)(1-R_0) \tag{6}$$

All of the Eigen values in the Jacobian matrix are manifestly negatives if and only if $R_0 < 1$. As a result, if $R_0 > 1$, the system is unstable; otherwise, it is locally asymptotically stable. As a result was verified [25].

VII. Endemic Equillibrium Equation for The Indian Pandemic COVID-19

We are now looking at the local asymptotic stability of the endemic equilibrium E_1. The Endemic equilibrium E_1 is locally asymptotically stable when R_0 is smaller than one. The Jacobian matrix of System Equn:(1) is provided by

$$J = \begin{bmatrix} -\beta I^* - \gamma & -\beta S^* & 0 & 0 \\ \beta I^* & \beta S^* - (\gamma+\theta+\alpha) & 0 & 0 \\ 0 & \theta & -(\gamma+\lambda) & 0 \\ 0 & \alpha & \lambda & -\gamma \end{bmatrix}$$

$| J - KI |=$

$$\begin{bmatrix} -\beta I^* - \gamma - k & -\beta S^* & 0 & 0 \\ \beta I^* & \beta S^* - (\gamma+\theta+\alpha) - k & 0 & 0 \\ 0 & \theta & -(\gamma+\lambda)-k & 0 \\ 0 & \alpha & \lambda & -\gamma-k \end{bmatrix}$$

The equation generated by equating to zero a system of equations' characteristic polynomial Equn:(1) near its endemic equilibrium E_2 is [25]

$$(k+\gamma)(k+\lambda+\gamma)(\lambda^2+\lambda(\frac{\beta}{(\gamma+\theta)}-1))(\gamma)(\gamma+\theta+\alpha)(1-R_0) = 0 \tag{7}$$

According to the equation, the roots that remain are quadratic polynomials roots, and the initial pair of roots are negative real values Equn:(5). It's additionally crucial to keep in mind that all parametric parameters are positives. We could deduce based on Routh- Hurwitz guidelines that the system Equn:(1) is asymptotically stable locally at its endemic equilibrium E_1.

VIII. Global stability analysis of SIQR model for COVID-19

In epidemiological models, achieving global stability is highly desirable because it indicates that the disease can be

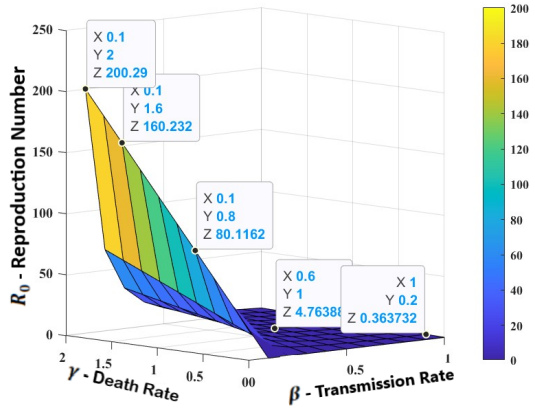

Fig. 2: Surface plot of R_0 for a variable value of β = 0 to 1

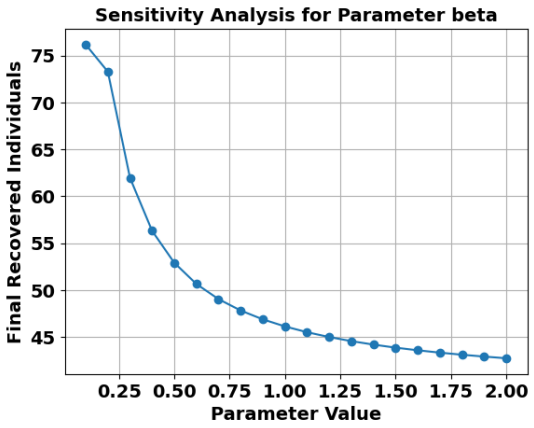

Fig. 3: Plot for R_0 for a fixed value of β = 0.8

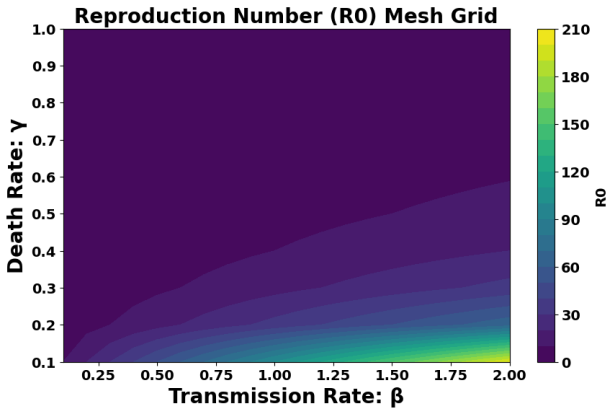

Fig. 4: Contour plot of R_0 as a function of β and γ

controlled or eradicated over the long term. This implies that with effective measures to prevent the initial spread or reintroduction of the disease, it can be eliminated permanently. The global stability of E_0 in system Equn:(1) is established by the following theorem.

Theorem 1. *If the value of R_0 is less than or equal to one, the system described by Equation:(1) in the model achieves global asymptotic stability.*

Proof: We will now proceed to construct the following Lyapunov function,

$$\mathscr{L}_1(S) = (S - S_0) - S_0 \log\left(\frac{S}{S_0}\right) \tag{8}$$

where $S_0 = \frac{\Lambda}{\gamma}$ corresponding to the E_0.
we obtain $\mathscr{L}_1 = 0 \iff S = S_0$.
By differentiating equation (8) with respect to t we get

$$\frac{\partial \mathscr{L}_1}{\partial t} = S' - \left(\frac{S_0}{S}\right) S'$$
$$\frac{\partial \mathscr{L}_1}{\partial t} = S' \left[1 - \left(\frac{S_0}{S}\right)\right]$$
$$\frac{\partial \mathscr{L}_1}{\partial t} = (\Lambda - \beta SI - \gamma S) \left[1 - \left(\frac{S_0}{S}\right)\right] \quad (9)$$
$$\frac{\partial \mathscr{L}_1}{\partial t} = (\Lambda - \beta SI - \gamma S) \left[1 - \left(\frac{\Lambda}{\gamma S}\right)\right]$$

where $S_0 = \frac{\Lambda}{\gamma}$

$$\frac{\partial \mathscr{L}_1}{\partial t} = (\Lambda - \beta SI - \gamma S) \left[\frac{\gamma S - \Lambda}{\gamma S}\right]$$
$$\frac{\partial \mathscr{L}_1}{\partial t} = \left[\frac{(\Lambda - \gamma S)^2}{\gamma S}\right] - \left(1 - \frac{\Lambda}{\gamma S}\right) \beta SI \leq 0$$

By applying the Lyapunov theorem, E_0 is globally asymptotically stable (g.a.s.). Next, the global stability E_1 in system Equn:(1) is demonstrated.

Theorem 2. *If the value of R_0 exceeds one, the system described by Equation: (1) becomes unstable within the specified domain.*

Proof: To demonstrate the global stability of E_1, we will attempt to construct the following Lyapunov function.

$$\mathscr{L}_2(M) = (M - M^*) - M^* \log\left(\frac{M}{M^*}\right) \quad (10)$$

where $M = S + I + Q + R$ and $M^* = S^* + I^* + Q^* + R^*$ By calculating the time derivative of $\mathscr{L}_2$ along the solutions of system (1), we obtain the following expression:

$$\frac{\partial \mathscr{L}_2}{\partial t} = M' \left(1 - \frac{M^*}{M}\right) \quad (11)$$
$$\frac{\partial \mathscr{L}_2}{\partial t} = [\Lambda - \gamma M] \left(1 - \frac{M^*}{M}\right)$$

where $M' = [\Lambda - \gamma M^*]$

$$\frac{\partial \mathscr{L}_2}{\partial t} = [\gamma M^* - \gamma M] \left(\frac{M - M^*}{M}\right)$$
$$\frac{\partial \mathscr{L}_2}{\partial t} = -\gamma [M - M^*] \left(\frac{M - M^*}{M}\right)$$
$$\frac{\partial \mathscr{L}_2}{\partial t} = -\gamma \left(\frac{(M - M^*)^2}{M}\right) \leq 0 \quad (12)$$

Therefore, it can be observed that $\frac{\partial \mathscr{L}_2}{\partial t}$ is negative and $\frac{\partial \mathscr{L}_2}{\partial t} = 0$ if and only if $S = S^*, I = I^*, Q = Q^*, R = R^*$ within domain 2 (Equn:(10)). Consequently, the singleton set E_1 is the largest positively invariant set contained within $(S, I, Q, R) \in Equn : (1)$ and $\mathscr{L}_2 = 0$ By the Lyapunov-LaSalle theorem, we can conclude that E_1 is globally asymptotically stable (g.a.s.).

IX. COVID-19 Sensitivity Analysis in INDIA

It is determined in this component if changing parameter values affect the functional value of the fertility number. Determining the crucial parameter that may function as a critical threshold for illness treatment is essential. R_0's sensitivity index to β, γ, α, θ be as follows [25]

$$\frac{\partial R_0}{\partial \beta} = \frac{\Lambda}{\gamma(\gamma + \theta + \alpha)}$$

$$\frac{\partial R_0}{\partial \gamma} = \frac{-\beta\Lambda(2\gamma + \theta + \alpha)}{(\gamma(\gamma + \theta + \alpha))^2}$$

$$\frac{\partial R_0}{\partial \theta} = \frac{-\beta\Lambda\gamma}{(\gamma(\gamma + \theta + \alpha))^2}$$

$$\frac{\partial R_0}{\partial \alpha} = \frac{-\beta\Lambda\gamma}{(\gamma(\gamma + \theta + \alpha))^2}$$

Because partial derivatives of beta are positive, raising any of the preceding elements raises the basic reproductive number R_0. The proportionate response to proportional stimulation can be used to determine elasticity.

$$E_\beta = \frac{\beta}{R_0}\left(\frac{\partial R_0}{\partial \beta}\right) = \frac{\beta}{R_0}\left(\frac{\Lambda}{\gamma(\gamma+\theta+\alpha)}\right) = 1$$
$$E_\gamma = \frac{\gamma}{R_0}\left(\frac{\partial R_0}{\partial \gamma}\right) = \frac{\gamma}{R_0}\left(\frac{-\beta\Lambda(2\gamma+\theta+\alpha)}{(\gamma(\gamma+\theta+\alpha))^2}\right) = -1.83$$
$$E_\theta = \frac{\theta}{R_0}\left(\frac{\partial R_0}{\partial \theta}\right) = \frac{\theta}{R_0}\left(\frac{-\beta\Lambda\gamma}{(\gamma(\gamma+\theta+\alpha))^2}\right) = -1.00166$$
$$E_\alpha = \frac{\alpha}{R_0}\left(\frac{\partial R_0}{\partial \alpha}\right) = \frac{\alpha}{R_0}\left(\frac{-\beta\Lambda\gamma}{(\gamma(\gamma+\theta+\alpha))^2}\right) = -1.1646 \quad (13)$$

From the above system of equationsE_β is positive, while

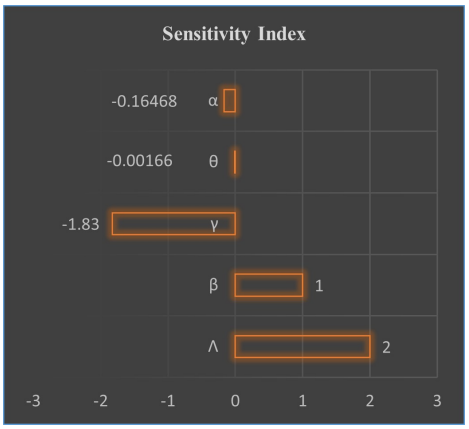

Fig. 5: Sensitivity index of R_0 against various parameter

E_γ,E_θ,E_α. It's all negative. This clearly illustrates that raising the value of β will result in an increase in the value of R_0. While increasing the value of γ, θ, α will decrease the value of R_0, A highly susceptible factor should be thoroughly investigated since minor modifications in the structure of the system may result in large quantitative changes in R_0.

X. Formation of SIQR Model With Synchronization

The slave system tracks the master system's trajectories as part of SIQR system with synchronization. However, it can be rephrased as the stabilization of the trajectories of a nonlinear system representing a difference between [31] two dynamics system. If one of the systems is master, and the other one is slave. Using the optimal control techniques, we

may adjust the slave system's response to synchronize [31] with the master SIQR system. These functions only affect the slave system and have no effect on SIQR system response of the master, first we define a master system [31].

$$\begin{aligned}\dot{S_1} &= \Lambda - \beta S_1 I_1 - \gamma S_1 - c_1 u_1(t)\\ \dot{I_1} &= \beta S_1 I_1 - (\gamma+\theta+\alpha) I_1 + c_1 u_2(t)\\ \dot{Q_1} &= \theta I_1 - (\lambda+\gamma) Q_1 + c_1 u_3(t)\\ \dot{R_1} &= \alpha I_1 + \lambda Q_1 - \gamma R_1 - c_1 u_4(t)\end{aligned} \tag{14}$$

However, we define a slave system as follows

$$\begin{aligned}\dot{S_2} &= \Lambda - \beta S_2 I_2 - \gamma S_2 - c_2 u_1(t)\\ \dot{I_2} &= \beta S_2 I_2 - (\gamma+\theta+\alpha) I_2 + c_2 u_2(t)\\ \dot{Q_2} &= \theta I_2 - (\lambda+\gamma) Q_2 + c_2 u_3(t)\\ \dot{R_2} &= \alpha I_2 + \lambda Q_2 - \gamma R_2 - c_2 u_4(t)\end{aligned} \tag{15}$$

The control signals are represented by the unknown terms u_1, u_2, u_3, u_4. This type of dynamical system can be defined as the distinction between master and slave [31].

$$(\dot{e_S}, \dot{e_I}, \dot{e_Q}, \dot{e_R}) = (\dot{S_2} - \dot{S_1}, \dot{I_2} - \dot{I_2}, \dot{Q_2} - \dot{Q_2}, \dot{R_2} - \dot{R_2}) \tag{16}$$

The study of error dynamical systems resulted in the creation of our time delay correlative synchronization controller [31].

$$\begin{aligned}\dot{e_S} &= (\Lambda - \beta S_1 I_1 - \gamma S_1 - c_1 u_1(t)) \\ &\quad -(\Lambda - \beta S_2 I_2 - \gamma S_2 - c_2 u_1(t))\\ \dot{e_I} &= (\beta S_1 I_1 - (\gamma+\theta+\alpha) I_1 + c_1 u_2(t)) \\ &\quad -(\beta S_2 I_2 - (\gamma+\theta+\alpha) I_2 + c_2 u_2(t))\\ \dot{e_Q} &= (\theta I_1 - (\lambda+\gamma) Q_1 + c_1 u_3(t)) \\ &\quad -(\theta I_2 - (\lambda+\gamma) Q_2 + c_2 u_3(t))\\ \dot{e_R} &= (\alpha I_1 + \lambda Q_1 - \gamma R_1 - c_1 u_4(t)) \\ &\quad -(\alpha I_2 + \lambda Q_2 - \gamma R_2 - c_2 u_4(t))\end{aligned} \tag{17}$$

then

$$\begin{aligned}\dot{e_S} &= (S_2 - S_1)[\beta(I_2 - I_1) + \gamma] + (c_1 - c_2) u_1(t)\\ \dot{e_I} &= (I_2 - I_1)[\beta(S_2 - S_1) + (\gamma+\theta+\alpha)] \\ &\quad +(c_1 - c_2) u_2(t)\\ \dot{e_Q} &= \theta(I_2 - I_1) - [(\lambda+\gamma)(Q_2 - Q_1)] \\ &\quad +(c_1 - c_2) u_3(t)\\ \dot{e_R} &= \alpha(I_2 - I_1)[\lambda(Q_2 - Q_1) - \gamma(R_2 - R_1)] \\ &\quad +(c_1 - c_2) u_4(t)\end{aligned} \tag{18}$$

We define active control functions $u_1(t)$, $u_2(t)$, $u_3(t)$ and $u_4(t)$ as [31].

$$\begin{aligned}(c_1 - c_2) u_1(t) &= V_S - (S_2 - S_1)(I_2 - I_1)\beta\\ (c_1 - c_2) u_2(t) &= V_I - (S_2 - S_1)(I_2 - I_1)\beta\\ (c_1 - c_2) u_3(t) &= V_Q - (I_2 - I_1)\theta\\ (c_1 - c_2) u_4(t) &= V_R - (I_2 - I_1)\alpha - (Q_2 - Q_1)\lambda\end{aligned} \tag{19}$$

$$\begin{aligned}\dot{e_S} = (S_2 - S_1)\gamma + V_S &= \gamma e_S + V_S\\ \dot{e_I} = (I_2 - I_1)(\gamma+\alpha+\theta) + V_I &= (\gamma+\alpha+\theta) e_I + V_I\\ \dot{e_Q} = -(Q_2 - Q_1)(\gamma+\lambda) + V_Q &= -(\gamma+\lambda) e_Q + V_Q\\ \dot{e_R} = -(R_2 - R_1)\gamma + V_R &= -\gamma e_R + V_R\end{aligned} \tag{20}$$

The terms V_S, V_I, V_Q and V_R are the linear function of the error terms e_S, e_I, e_Q and e_R with the choice of u_1,u_2,u_3 and u_4 the error system between the master and slave system becomes [31].

$$\begin{aligned}\dot{e_S} &= \gamma e_S + V_S\\ \dot{e_I} &= (\gamma+\alpha+\theta) e_I + V_I\\ \dot{e_Q} &= -(\gamma+\lambda) e_Q + V_Q\\ \dot{e_R} &= -\gamma e_R + V_R\end{aligned} \tag{21}$$

In fact, we do not solve the above equations if the solution converges to zero, Therefore the control terms $V_S(e_S)$,$V_I(e_I)$,$V_Q(e_Q)$ and $V_R(e_R)$ can be chosen such that the above system of equations becomes stable with zero steady state [31].

$$\begin{pmatrix} V_S \\ V_I \\ V_Q \\ V_R \end{pmatrix} = A \begin{pmatrix} e_S \\ e_I \\ e_Q \\ e_R \end{pmatrix} \tag{22}$$

Where A is a 4 x 4 real matrices so that all the eigen value of λ_i of the above system satisfy the following condition [31].

$$|\, arg(\lambda_i)\, | > \frac{\alpha\pi}{2} \tag{23}$$

we choose

$$A = \begin{bmatrix} \gamma - k & 0 & 0 & 0 \\ 0 & (\gamma+\theta+\alpha) - k & 0 & 0 \\ 0 & 0 & -(\gamma+\lambda) - k & 0 \\ 0 & 0 & 0 & -\gamma - k \end{bmatrix}$$

The eigen values of the linear system Equn:(22) are equal (-k, -k, -k, -k) which is enough to satisfy the necessary and sufficient condition of Equn:(23). In order to compare the obtained result with that of the master–slave synchronization scheme $u_1(t)$, $u_2(t)$, $u_3(t)$ and $u_4(t)$. When a fault error in Figures:(6-9) occurs, the master–slave synchronization error shown in Figures:(6-9). Moreover, the master is the controlling device that initiates and coordinates the actions of the other devices, known as slaves. Slaves are devices that are controlled by the master. They follow the commands or signals provided by the master device. Synchronization error occurs when there is a mismatch or timing issue in the communication or coordination between the master and slave devices. For example, if the master expects a response from a slave at a certain time and the slave does not respond within that time frame, a synchronization error may occur. Now, a Figures:(6-9) illustrating master and slave synchronization errors might include timelines or sequences of events. It

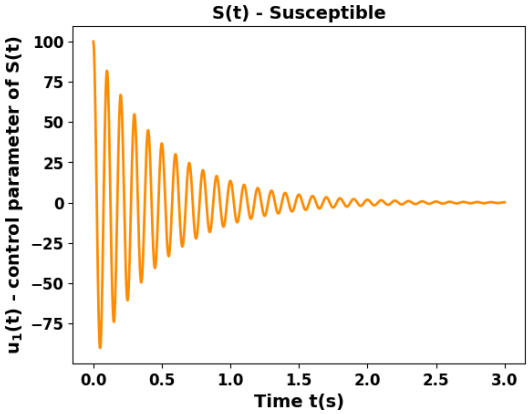

Fig. 6: Synchronization error with fault $u_1(t)$

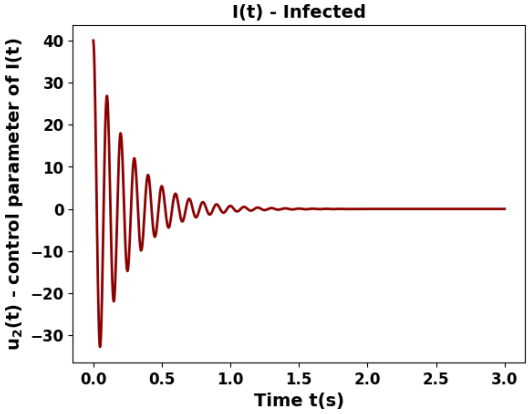

Fig. 7: Synchronization error with fault $u_2(t)$

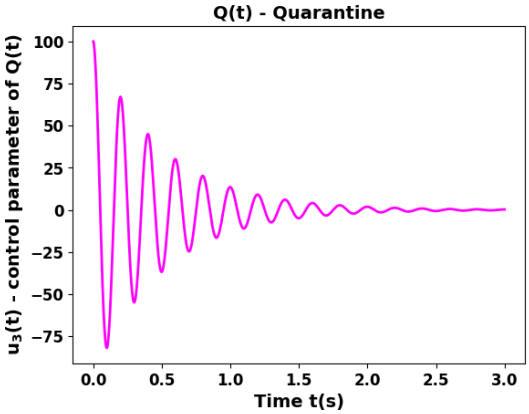

Fig. 8: Synchronization error with fault $u_3(t)$

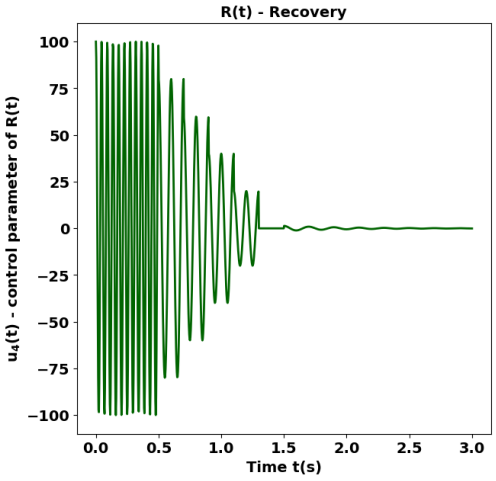

Fig. 9: Synchronization error with fault $u_4(t)$

could show when the master sends a command, when the slave is supposed to respond, and any discrepancies or errors that occur. The diagram might also depict factors like delays, disruptions, or conflicts that lead to synchronization errors[31].

XI. COVID-19 Indian Pandemic: Optimal Control

The prevention and control effort, such as the use of facial masks by society, demonstrates an overall health awareness campaign to educate people about the importance of facial masks in avoiding COVID-19 transmission. The evaluation attempt indicates efforts such as handwashing to avoid infection, as well as maintaining distance. Through the use of online platforms, radio, TV, and conventional communal legitimacy, the public health awareness responsibility aims to educate the public about the significance of maintaining social distance and washing their hands. The measures employed to isolate those who were exposed to people with the infection involve recruiting and instructing healthcare providers to use protective clothing and footwear (PPE) [22], recording the contact information of those exposed to COVID-19 via home inspections and calls, providing psychotherapy, offering emergency vehicles for transporting people with the infection to quarantine centers, conducting general/COVID-19 examinations, providing isolation centers for medical care, and other related activities [30].

$$\begin{aligned} \tfrac{dS}{dt} &= \Lambda - \beta S I u_1(t) - \gamma S \\ \tfrac{dI}{dt} &= \beta S I u_1(t) - (\gamma + \theta + \alpha) I \\ \tfrac{dQ}{dt} &= \theta I - (\lambda + \gamma) Q + u_2(t) R \\ \tfrac{dR}{dt} &= \alpha I + \lambda Q - (\gamma + u_2(t)) R \end{aligned} \tag{24}$$

$$K[u_1(t), u_2(t)] = \int_0^{t_\alpha} [I(t) + \frac{1}{2} C_1 {u_1}^2(t) + \frac{1}{2} C_2 {u_2}^2(t)] dt \tag{25}$$

The set of differential Equn:(1), subject to all control efforts $u_1(t)$, $u_2(t)$, are considered to be limited and time-dependent Lebesgue functions on the interval $(0, t)$, where t is the final time. The set of control efforts is defined as

$$\Phi = (u_1(t), u_2(t) | 0 \leq u_1(t), u_2(t) \leq 1, (0 \leq t \leq t_\alpha))$$

The variables C_1 and C_2 are the cost-balancing factors for the use of a facial mask (u_1), efforts of soaping hands to avoid infection, as well as distance (u_2), accordingly. The expressions suggest the costs for the use of a facial mask, efforts of soaping hands to avoid infection, as well as distance, in that order. Due to the research on optimal epidemic administration, the cost of the controls is deemed to be nonlinear and quadratic [29, 30]. If $u_1 = u_2 = 1$, then at time t, 100% effort is put into the use of a facial mask and efforts of soaping hands to avoid infection, respectively [28]. If $u_1 = u_2 = 0$, then there is no use of a facial mask and efforts of soaping hands to avoid infection, no isolation for the infected non-hospitalized individuals, and no handwashing[33].

This section will look at the control time-dependent parameters. Our aim is to find an optimal control for the use of a facial mask u_1 and efforts of soaping hands to avoid infection u_2, such that

$$K[u_1^*(t), u_2^*(t)] = \min_{(u_1(t), u_2(t) \in \phi)} K[u_1(t), u_2(t)] \tag{26}$$

Applying Pontryagin's Maximum Principle to the COVID-19 model of Equn:(3) yields the required conditions that an optimum solution must meet. This concept transforms system Equn:(3) and Equn:(14) into a problem of minimizing the pointwise Hamiltonian, H_1, which is denoted as:

$$\begin{aligned} U &= (I, u_1(t), u_2(t), \tau_1, \tau_2, \tau_3, \tau_4) \\ U &= L\left[I, u_1(t), u_2(t), \tau_1\left(\frac{dS}{dt}\right), \tau_2\left(\frac{dI}{dt}\right), \tau_3\left(\frac{dQ}{dt}\right), \tau_4\left(\frac{dR}{dt}\right)\right] \end{aligned} \tag{27}$$

$$\begin{aligned} H = [I(t) &+ \frac{1}{2} C_1 {u_1}^2(t) + \frac{1}{2} C_2 {u_2}^2(t)] \\ &+ \tau_1(\Lambda - \beta S I u_1(t) - \gamma S) \\ &+ \tau_2(\beta S I u_1(t) - (\gamma + \theta + \alpha) I) \\ &+ \tau_3(\theta I - (\lambda + \gamma) Q + u_2(t) R) \\ &+ \tau_4(\alpha I + \lambda Q - (\gamma + u_2(t)) R) \end{aligned} \tag{28}$$

Let τ_i, where $i = 1, 2, 3, ...,$ denotes the related costate variables for the state variables S, I, Q, R. The following theorem is stated using Equn:(7).

Theorem 3. *Given an optimum control $u_1^*(t)$, $u_2^*(t)$, and solutions $S_1^0(t)$, $I_1^0(t)$, $Q_1^0(t)$, $R_1^0(t)$ of the related state system Equn:(1) that minimize $U(t)$, costate variables exist that satisfy the following systems of equations.*

$$\begin{aligned} \dot{\tau_1} &= (\tau_1 - \tau_2)\beta u_1 I + \tau_1 \gamma \\ \dot{\tau_2} &= (\tau_1 - \tau_2)\beta u_1 S + (\tau_2 - \tau_3)\theta \\ &\quad - (\tau_2 - \tau_4)\alpha + \tau_2 \gamma \\ \dot{\tau_3} &= (\tau_3 - \tau_4)\lambda + \tau_3 \gamma \\ \dot{\tau_4} &= (\tau_4 - \tau_3)u_2 + \tau_4 \gamma \end{aligned} \tag{29}$$

the transversely conditions were satisfied by the adjoint variables

$$\tau_1(t_\alpha) = 0, \tau_2(t_\alpha) = 0, \tau_3(t_\alpha) = 0, \tau_4(t_\alpha) = 0 \quad t \in t_\alpha$$

the optimality conditions are also listed.

$$\begin{aligned} u_1^*(t) &= \max\left\{0, \min\left(\tfrac{\beta S^* I^* (\tau_1 - \tau_2)}{C_1}\right)\right\} \\ u_2^*(t) &= \max\left\{0, \min\left(\tfrac{Q^* (\tau_3 - \tau_4)}{C_2}\right)\right\} \end{aligned}$$

The differential equations regulating the costate variables are found by differentiating the Hamiltonian function, H, at the corresponding solutions of equations Equn:(3) and the optimum control with final time conditions.We try to minimize the Hamiltonian using the control variable $u_1^*(t)$, $u_2^*(t)$. Moreover, the Hamiltonian is linear in the control parameter. If we consider the optimal control is singular, then the switching function as

For various values of u_1 (0.02,0.04,0.05,0.06 and 0.1), Fig: (10-13) represent the optimal control graph for usage of a facial mask and no efforts of soaping of hands.

For various values of u_2 (0.02,0.04,0.05,0.06 and 0.1), Fig: (14-17) represent the optimal control graph for no usage of a facial mask and efforts of soaping of hands.

$$\begin{aligned}
\dot{\tau_1} &= -\frac{\partial U}{\partial S} = (\tau_1 - \tau_2)\beta u_1 I + \tau_1\gamma \\
\dot{\tau_2} &= -\frac{\partial U}{\partial I} = (\tau_1 - \tau_2)\beta u_1 S + (\tau_2 - \tau_3)\theta \\
&\quad -(\tau_2 - \tau_4)\alpha + \tau_2\gamma \\
\dot{\tau_3} &= -\frac{\partial U}{\partial Q} = (\tau_3 - \tau_4)\lambda + \tau_3\gamma \\
\dot{\tau_4} &= -\frac{\partial U}{\partial R} = (\tau_4 - \tau_3)u_2 + \tau_4\gamma
\end{aligned} \tag{30}$$

This yields the costate system in Equn:(13). The optimality requirements are specified in the interior of the control set.

$$\Phi = (u_1(t), u_2(t) | 0 \leq u_1(t), u_2(t) \leq 1, (0 \leq t \leq t_\alpha))$$

$$\begin{aligned}
\frac{\partial H_1}{\partial U_1} &= C_1 u_1 - \tau_1\beta SI + \tau_2\beta SI \\
\frac{\partial H_1}{\partial U_1} &= C_2 u_2 - \tau_3 Q + \tau_4 R
\end{aligned} \tag{31}$$

solving $u_1(t)$ as $u_1^*(t)$ and $u_2(t)$ as $u_2^*(t)$, then we get

$$\begin{aligned}
u_1^*(t) &= \frac{(\tau_1-\tau_2)\beta S^0 I^0}{C_1} \\
u_2^*(t) &= \frac{(\tau_3-\tau_4)Q^0}{C_2}
\end{aligned} \tag{32}$$

Equn:(29) gives the optimal control efforts in compact form, utilizing the boundaries of the controls $u_1^*(t)$ and $u_2^*(t)$. The optimality system is given by Equn:(1), Equn:(26), together with the optimality requirements Equn:(29)), the initial conditions S_1^0, I_1^0, Q_1^0 and R_1^0 final time conditions Equn:(28). Due to the a priori boundedness of the state variables, costate functions, and the resulting Lipschitz structure of the ODEs, the uniqueness of the optimality system solutions is obtained for the small-time interval $t \in t_\alpha$.

XII. COVID-19 Indian Epidemic Numerical Analysis

We performed numerical modelling to examine the effects of public education, quarantine, and handwashing, as well as the fraction of exposed people who will be restricted. This was carried out employing parameter values and initial conditions from the COVID-19, SARS, and MERS literature [30]. We initiated numerical simulations by considering the values of the parameters in Table:(II). Since β is the disease-induced mortality rate and γ is the natural death rate, we may deduce that $\beta < \gamma$. As a starting point, consider these traits along with the essential prerequisites.The following are the initial conditions for the state variables: $S(0) = 2$, $I(0) = 0$, $Q(0) = 0$ and $R(0) = 0$,We numerically solve our proposed model Equn:(1). The numerical result is validated when $R_0 < 1$, and the solutions of model Equn:(1) converge to the DFE, as illustrated in Fig: 2.

The forward backward sweep strategy is used to solve the optimality system. Lenhart and Workman [30] describe the scheme's specifics. Many researchers have calculated different values of the basic reproduction number for person-to-person transmission, reservoir-to-person transmission, and environmental transmission, and their results have been compared with other types of coronaviruses, SARS, and MERS, showing almost identical results [26, 29]. As a result, we concentrate our numerical simulation on the influence of various combinations of control interventions with varying control profiles on the transmission dynamics of COVID-19[33].

Fig:18-21 The solution curves for the model Fig:(1) at disease free equilibrium point. Fig:(19-22) shows the numerical results of the system Fig:(1) when $R_0 < 1$. These figures show that all numerical solutions for the problem converged to the disease-free equilibrium $E_0 = (1.1, 0.82, 0, 0.08)$ for the case $R_0 > 1$.

Fig:(22-25) The solution curves for the model Fig:(1) at Endemic Equilibrium point. Fig:(22-25). Dynamical phenomena around Endemic Equilibrium. When $R_0 > 1$ the numerical results of the system Fig:(1) are depicted in Fig:(4). These figures show that all numerical solutions converged to the Endemic equilibrium.$E^*(0.234, 3.134, 0.005, 0.6201)$ for the case $R_0 > 1$.

XIII. Result and Discussion

We conducted numerical modeling to assess the impacts of public education, quarantine measures, handwashing, and the restriction of the fraction of exposed individuals. This analysis utilized parameter values and initial conditions derived from existing literature on COVID-19, SARS, and MERS [30]. The aim is to provide a comprehensive understanding of how these interventions, informed by previous research, influence the dynamics of infectious diseases and contribute to effective control strategies. We begin numerical simulations by considering the values of the parameters in Table:(**??**). Since β is the disease-induced mortality rate and γ is the natural death rate, we may deduce that $\beta > \gamma$. As a starting point, consider these traits as well as the essential prerequisites. The following are the beginning conditions for the state variables: $S_0 = 2$, $I_0 = 0$, $Q_0 = 0$, and $R_0 = 0$. We numerically solve our proposed model Equn:(1). The numerical result is validated when $R_0 < 1$ and the solutions of model Equn:(1) converge to the DFE.

The surface plot of R_0 (basic reproduction number) for a variable value of the beta (β) parameter provides a visual representation of how changes in the transmission rate influence the potential spread of an infectious disease shown in (Fig:2). The surface plot visually illustrates the relationship between R_0 and varying values of the β parameter. The x-axis typically represents the β values, the y-axis represents other relevant parameters, and the z-axis corresponds to the resulting R_0 values. When the surface plot is generated, it allows researchers and epidemiologists to observe how changes in the transmission rate (β) impact the overall transmission potential of the disease. A steeper upward slope on the surface plot indicates a higher R_0, suggesting a greater likelihood of widespread transmission. Conversely, a flatter slope signifies lower transmission potential. This type of visualization is invaluable in understanding the sensitivity of R_0 to changes in the transmission rate, helping

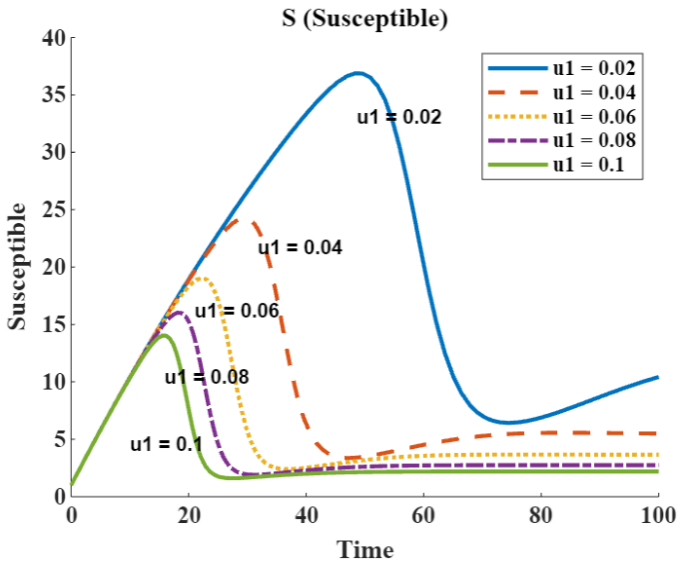

Fig. 10: For various values of u_1 (0.02,0.04,0.05,0.06 and 0.1) at susceptible rate.

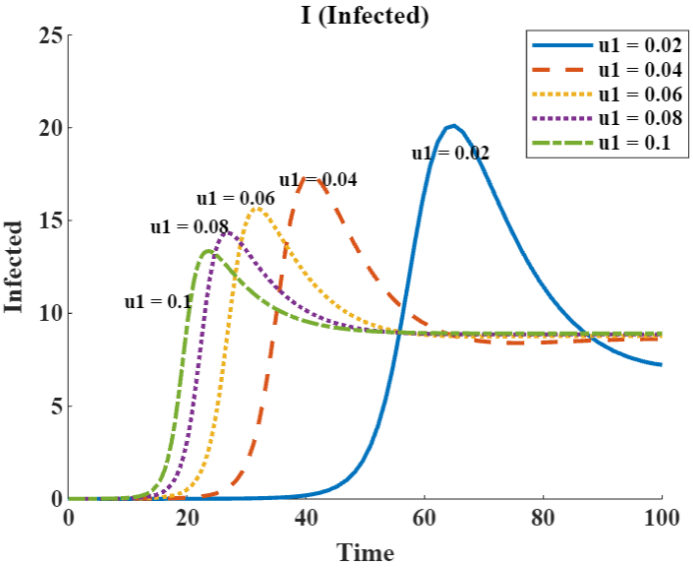

Fig. 11: For various values of u_1 (0.02,0.04,0.05,0.06 and 0.1) at infected rate.

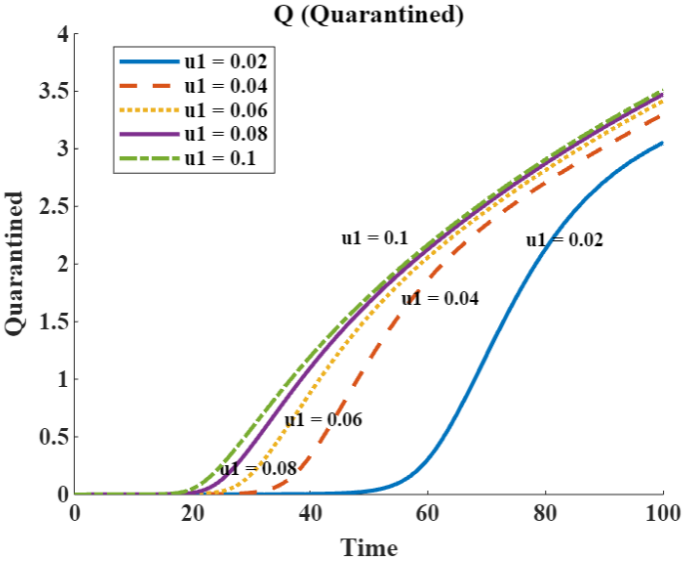

Fig. 12: For various values of u_1 (0.02,0.04,0.05,0.06 and 0.1) at quarantine rate.

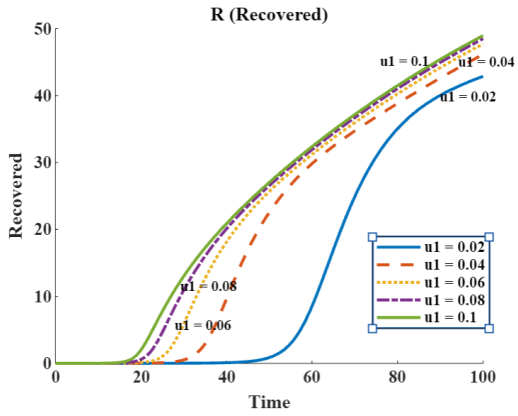

Fig. 13: For various values of u_1 (0.02,0.04,0.05,0.06 and 0.1) at recovery rate.

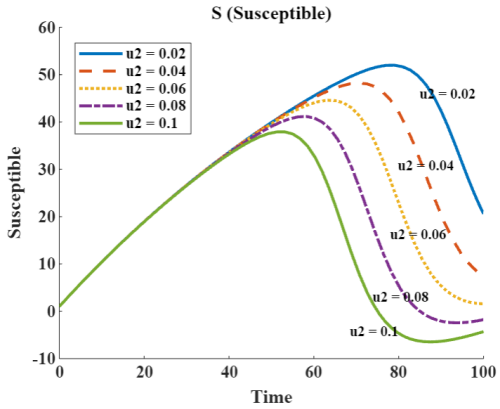

Fig. 14: For various values of u_2 (0.02,0.04,0.05,0.06 and 0.1) at susceptible rate.

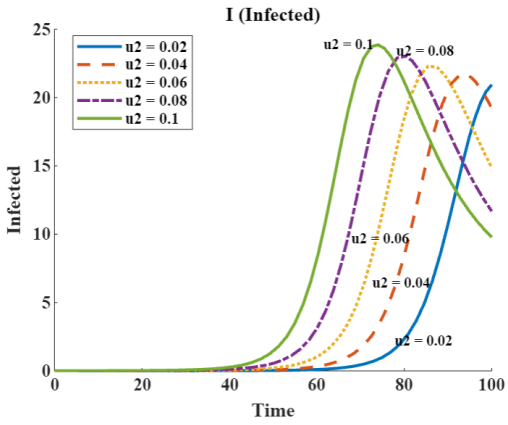

Fig. 15: For various values of u_2 (0.02,0.04,0.05,0.06 and 0.1) at infected rate.

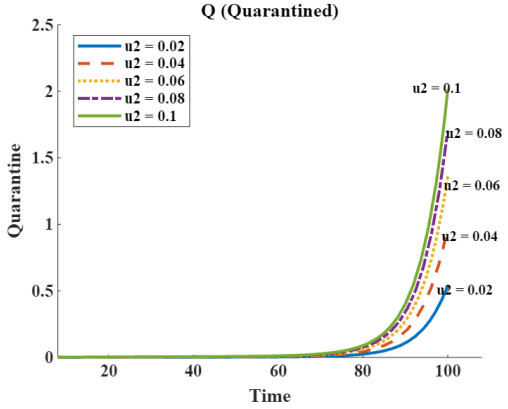

Fig. 16: For various values of u_2 (0.02,0.04,0.05,0.06 and 0.1) at quarantine rate.

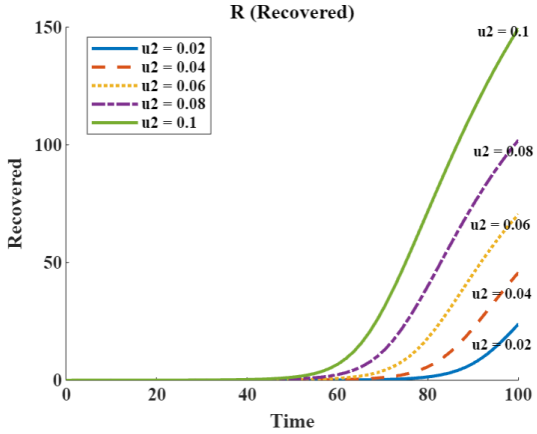

Fig. 17: For various values of u_2 (0.02,0.04,0.05,0.06 and 0.1) at recovery rate.

TABLE II: PARAMETER MEANINGS FOR MODEL

Parameters	Description	Values/Range	Reference
Λ	Recruitment Rate	2	assumed
β	Disease Transmission Rate from S to I	1.05 /day	[11]
θ	Disease Transmission Rate from I to Q	0.001 /day	[11]
α	Recovery Rate from I to R	0.9871 /day	[25]
λ	Recovery Rate from Q to R	0.1243 /day	[25]
γ	Natural Death Rate	0.5	[11]

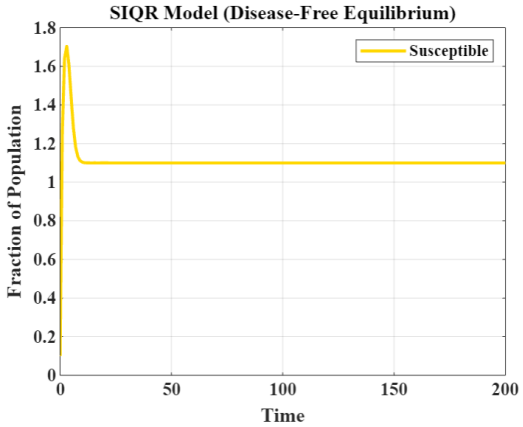

Fig. 18: Plot for change in susceptible rate at disease free equilibrium point.

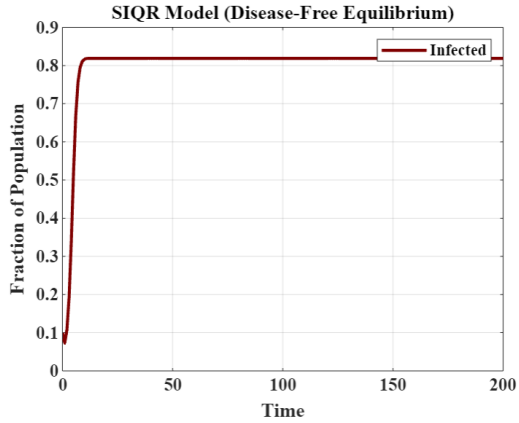

Fig. 19: Plot for change in infected rate at disease free equilibrium point.

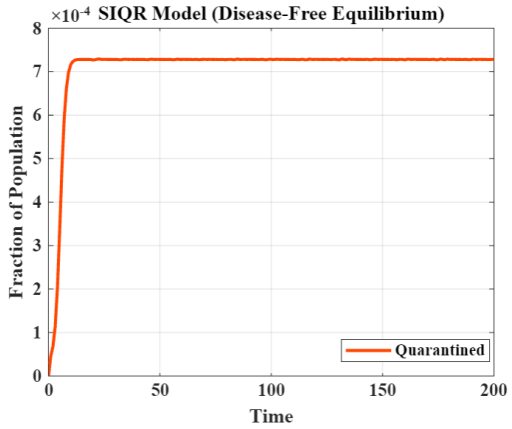

Fig. 20: Plot for change in quarantine rate at disease free equilibrium point.

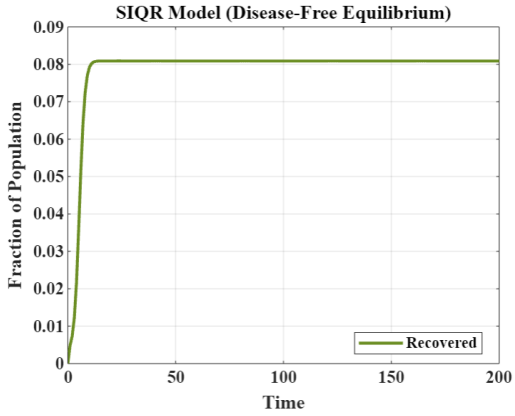

Fig. 21: Plot for change in recovery rate at disease free equilibrium point.

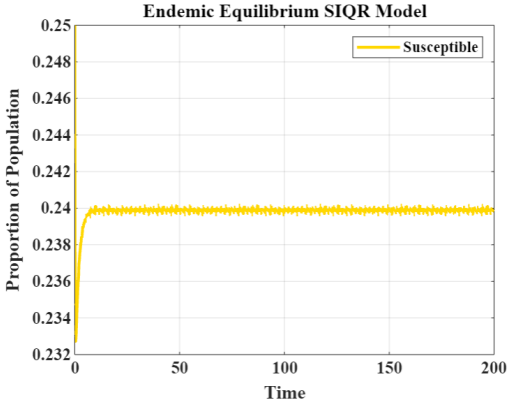

Fig. 22: Plot for change in susceptible rate at endemic equilibrium point.

researchers make informed decisions about interventions and control measures to mitigate the spread of infectious diseases. It provides a dynamic and intuitive representation of the complex relationship between transmission parameters and disease dynamics.

The forward-backward sweep strategy stands as the chosen method for solving the optimality system, with its details outlined by Lenhart and Workman [30]. This strategic approach is employed to navigate the intricacies of the optimality system efficiently. Numerous researchers have undertaken the calculation of distinct values for the basic reproduction number, considering diverse transmission modes such as person-to-person, reservoir-to-person, and environmental transmission. Comparisons have been drawn between these values and those associated with other coronaviruses like SARS and MERS, revealing striking similarities [26, 29].

In light of the consistent findings across various transmission modes and coronaviruses, our numerical simulations hone in on a specific focus. We direct our attention to exploring the impact of diverse combinations of control interventions, each characterized by distinct control profiles, on the transmission dynamics of COVID-19. This targeted approach aims to unravel the nuanced interactions between different control measures and their effectiveness in shaping the trajectory of COVID-19 transmission. The change in the SIQR (Susceptible-Infectious-Quarantined-Recovered) rate at the disease-free equilibrium point refers to how the rate of individuals transitioning through the SIQR compart-

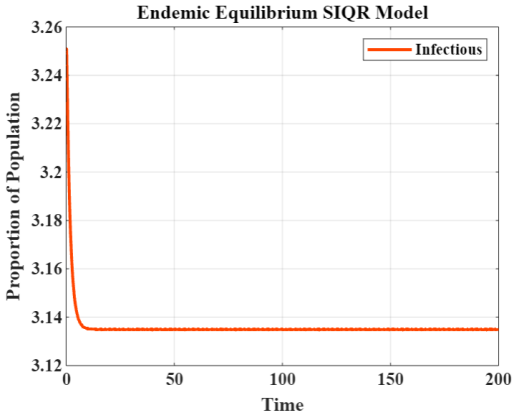

Fig. 23: Plot for change in infected rate at endemic equilibrium point.

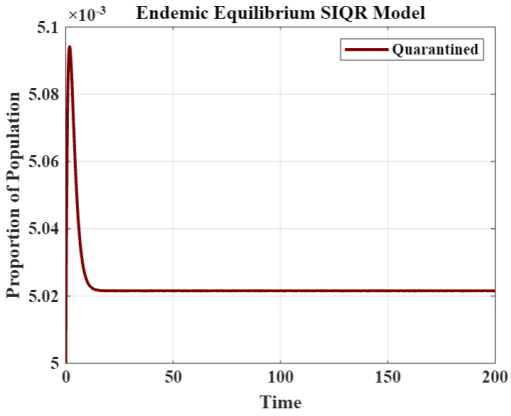

Fig. 24: Plot for change in quarantine rate at endemic equilibrium point.

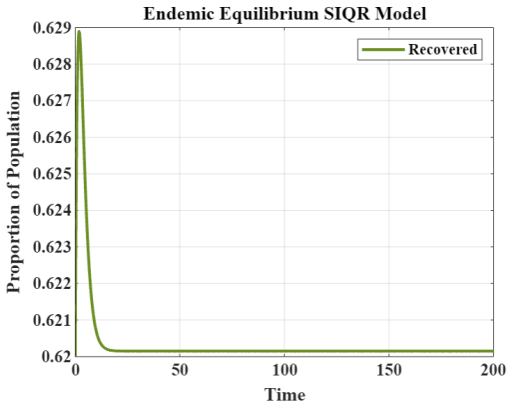

Fig. 25: Plot for change in recovery rate at endemic equilibrium point.

ments evolves when there is no active infection present in the population.

The SIQR model is a compartmental model used to represent the dynamics of an infectious disease within a population. It divides individuals into different compartments based on their disease status: Susceptible (S), Infectious (I), Quarantined (Q), and Recovered (R) shown in Figs. 9. This is a state in the model where no individuals are actively infected. At this point, all individuals are in the susceptible state, and there is no ongoing transmission of the disease. The rate of change in the SIQR compartments signifies how the numbers of individuals in each compartment are evolving over time.

In this context, attention is directed towards the rate of change within the SIQR compartment. The alteration in the rate of change within the SIQR compartment at the disease-free equilibrium point is affected by diverse factors, including the efficacy of interventions, control measures, or variations in model parameters. As an illustration, the rate might be influenced by the effectiveness of quarantine measures, public health campaigns, or vaccination strategies. The examination of the alteration in the SIQR rate offers insights into the dynamic behavior of the model in the absence of continuous. It helps to understand how the population responds to different scenarios and interventions in maintaining a disease-free state. Understanding the change in the SIQR rate at the disease-free equilibrium point is crucial for optimizing control strategies as shown in (Fig:18-25). Researchers and

policymakers can use this information to identify effective measures that contribute to preventing the resurgence of infections and maintaining a disease-free state. In summary, the change in the SIQR rate at the disease-free equilibrium point offers valuable insights into the responsiveness of the population to interventions and control measures when the infectious disease is not actively spreading. It aids in formulating strategies to keep the disease under control and prevent its re-emergence within the community.

XIV. Conclusion

This research article presents a detailed analysis of the SIQR mathematical model augmented with an optimal control strategy aimed at mitigating the spread of infectious diseases, specifically targeting the COVID-19 pandemic. The model incorporates two control measures, represented by u_1 and u_2, corresponding to the use of face masks and the effectiveness of handwashing, respectively. By integrating these control variables into the model, the researchers aim to evaluate their efficacy in reducing disease transmission.

The baseline scenario assumes a high initial transmission rate, represented by $R_0 = 16.67$, indicative of a rapidly spreading infectious agent. However, the model identifies an endemic equilibrium state characterized by stable values of susceptible, infected, quarantined, and recovered populations (S^*, I^*, Q^*, R^*). These equilibrium values ($S^* = 0.23$, $I^* = 3.13$, $Q^* = 0.005$, $R^* = 0.62$) provide valuable insights into the long-term dynamics of the disease within the population.

The introduction of the optimal control strategy, leveraging the use of face masks and handwashing, yields promising results in reducing disease spread. Through mathematical simulations, the researchers demonstrate that the application of these control measures leads to a significant reduction in the rate of infection, effectively curbing the epidemic trajectory. This underscores the importance of proactive interventions and individual behaviors in controlling infectious disease outbreaks.

Furthermore, the study explores the implementation of a synchronization method of control, employing master and slave equations to coordinate and optimize control efforts across different regions or populations. By synchronizing control measures, the researchers aim to enhance the overall effectiveness of disease containment strategies, particularly in scenarios involving interconnected or geographically dispersed communities.

We conducted numerical modeling to assess the impacts of public education, quarantine measures, handwashing, and the restriction of the fraction of exposed individuals. This analysis utilized parameter values and initial conditions derived from existing literature on COVID-19, SARS, and MERS [30]. The aim is to provide a comprehensive understanding of how these interventions, informed by previous research, influence the dynamics of infectious diseases and contribute to effective control strategies. We begin numerical simulations by considering the values of the parameters in Table 2. Since β is the disease-induced mortality rate and γ is the natural death rate, we may deduce that $\beta > \gamma$. As a starting point, consider these traits as well as the essential prerequisites. The following are the beginning conditions for the state variables.

In conclusion, the research article highlights the efficacy of the SIQR mathematical model coupled with optimal control strategies in mitigating the spread of infectious diseases like COVID-19. The findings underscore the importance of proactive and coordinated control efforts, emphasizing the significant impact of individual behaviors and community-level interventions in containing epidemics. By leveraging mathematical modeling and control theory, the study provides valuable insights that can inform public health policies and interventions aimed at safeguarding population health and mitigating the impact of infectious disease outbreaks.

References

[1] D. Bernoulli, "Essai d'une nouvelle analyse de la mortalité causée par la petite vérole," Mem. Math. Phy. Acad. Roy. Sci. Paris, p. 145, 1760.

[2] B. Buonomo, A. d'Onofrio, and D. Lacitignola, "Global stability of an SIR epidemic model with information dependent vaccination," Math. Biosci., vol. 216, pp. 9-16, 2008.

[3] T. Chakraborty and I. Ghosh, "Real-time forecasts and risk assessment of novel coronavirus (COVID-19) cases: a data-driven analysis," Chaos Solitons Fractals, 2020, doi:10.1016/j.chaos.2020.109850.

[4] O. Diekmann, J. A. P. Heesterbeek, and J. A. J. Metz, "On the definition and the computation of the basic reproduction number ratio R_0 in models for infectious diseases in heterogeneous populations," J. Math. Biol., vol. 28, pp. 365-82, 1990.

[5] P. van den Driessche and J. Watmough, "Reproduction numbers and sub-threshold endemic equilibria for compartmental models of disease transmission," Math. Biosci., vol. 180, issues 1-2, pp. 29-48, Nov.-Dec. 2002, doi: https://doi.org/10.1016/S0025-5564(02)00108-6.

[6] D. Fanelli and F. Piazza, "Analysis and forecast of COVID-19 spreading in China, Italy and France," Chaos Solitons Fractals, vol. 134, p. 109761, 2020.

[7] G. Guckenheimer and P. Holmes, Nonlinear Oscillations, Dynamical Systems, and Bifurcations of Vector Fields. New York: Springer Verlag, 1983.

[8] T. K. Kar, S. K. Nandi, S. Jana, and M. Mandal, "Stability and bifurcation analysis of an epidemic model with the effect of media," Chaos Solitons Fractals, vol. 120, pp. 188-99, 2019.

[9] M. Manotosh, S. J. Mukherjee, S. K. Nandi, C. A. Khatu, and T. K. Kar, "A model based study on the dynamics of COVID-19: Prediction and control," 2020, doi: https://doi.org/10.1016/j.chaos.2020.109889.

[10] L. Li, C. H. Wang, S. H. Wang, M. T. Li, L. Yakob, B. Cazelles, Z. Jin, and W. Y. Zhang, "Hemorrhagic fever with renal syndrome in China: Mechanisms on two distinct annual peaks and control measures," 2018.

[11] H. M. Ahmed, R. A. Elbarkouky, O. A. M. Omar, and M. A. Ragusa, "Models for COVID-19 Daily Confirmed Cases in Different Countries," Mathematics, vol. 9, p. 659, 2021, doi: https://doi.org/10.3390/math9060659.

[12] A. O. A1, A. Karaoğlan, M. A. R3,4, and E. S.1, "Fractional Integral Inequalities via Atangana-Baleanu Operators for Convex and Concave Functions," Hindawi Journal of Function Spaces, vol. 2021, Article ID 1055434, 10 pages, doi: https://doi.org/10.1155/2021/1055434.

[13] K. Prem, Y. Liu, T. W. Russell, A. J. Kucharski, R. M. Eggo, and N. Davies, "The effect of control strategies to reduce social mixing on outcomes of the COVID-19 epidemic in Wuhan, China: a modelling study," The Lancet Public Health, 2020.

[14] W. O. Kermack and A. G. McKendrick, "Contributions to the mathematical theory of epidemics-i," Proc. R. Soc., vol. 115A, pp. 700-21, 1927.

[15] A. J. Krener, "The high order maximal principle and its application to singular extremals," SIAM J. Control Optim., vol. 15, no. 2, pp. 256-93, 1977.

[16] A. J. Kucharski, T. W. Russell, C. Diamond, Y. Liu, J. Edmunds, S. Funk, et al., "Early dynamics of transmission and control of COVID-19: a mathematical modelling study," Lancet Infect. Dis., 2020.

[17] U. Ledzewicz and H. Schättler, "On optimal singular controls for a general SIR-model with vaccination and treatment," Discrete Contin. Dyn. Syst., 2011(2): 981-90.

[18] S. Lenhart and J. T. Workman, Optimal Control Applied to Biological Models. CRC Press, 2007.

[19] L. Li, C. H. Wang, S. H. Wang, M. T. Li, L. Yakob, B. Cazelles, Z. Jin, and W. Y. Zhang, "Hemorrhagic fever with renal syndrome in China: Mechanisms on two distinct annual peaks and control measures," Int. J. Biomath., vol. 11, no. 2, 2018.

[20] Y. Liu, A. A. Gayle, A. Wilder-Smith, and J. Rocklöv, "The reproductive number of COVID-19 is higher compared to SARS coronavirus," J. Travel Med., 2020, pp. 1-4.

[21] G. O. Fosu, J. M. Opong, and J. K. Appati, "Construction of Compartmental Models for COVID-19 with Quarantine, Lockdown and Vaccine Interventions," SSRN, 2020, doi: http://dx.doi.org/10.2139/ssrn.3574020.
[22] T. D. Keno and H. T. Etana, "Optimal Control Strategies of COVID-19 Dynamics Model," Hindawi Journal of Mathematics, vol. 2023, Article ID 2050684, 20 pages, doi: https://doi.org/10.1155/2023/2050684.
[23] A. I. Kashif Butt, M. Imran, D. B. D. Chamaleen, and S. Batool, "Optimal control strategies for the reliable and competitive mathematical analysis of Covid-19 pandemic model," Math. Meth. Appl. Sci., vol. 46, issue 2, doi: https://doi.org/10.1002/mma.8593.
[24] M. D. Zamir, T. Abdeljawad, F. Nadeem, A. Wahid, and A. Yousef, "An Optimal control analysis of a COVID-19 model," Alexandria Eng. J., vol. 60, pp. 2875-2884, 2021.
[25] S. Boulaaras, R. Ramesh, and G. Arul Joseph, "SEIR model for COVID-19: stability of the standard coronavirus factor and control mechanism," Eur. Phys. J. Spec. Top., doi: https://doi.org/10.1140/epjs/s11734-023-00915-4.
[26] M. Rafiq, J. E. Macías-Díaz, A. Raza, and N. Ahmed, "Design of a nonlinear model for the propagation of COVID-19 and its efficient nonstandard computational implementation," Appl. Math. Comput., vol. 391, 2021, 126086, doi: https://doi.org/10.1016/j.amc.2020.126086.
[27] E. F. A. Obsu and S. F. Balcha, "Optimal control strategies for the transmission risk of COVID-19," J. Biol. Dyn., vol. 14, no. 1, pp. 590-607, 2020, doi: 10.1080/17513758.2020.1788182.
[28] C. E. Madubueze, S. Dachollom, and I. O. Onwubuya, "Controlling the Spread of COVID-19: Optimal Control Analysis," Hindawi Comput. Math. Methods Med., vol. 2020, Article ID 6862516, 14 pages, doi: https://doi.org/10.1155/2020/6862516.
[29] P. van den Driessche, "Reproduction numbers of infectious disease models," Infect. Dis. Model., vol. 2, pp. 288-303, 2017, doi: http://dx.doi.org/10.1016/j.idm.2017.06.002.
[30] L. L. Obsu and S. F. Balcha, "Optimal control strategies for the transmission risk of COVID-19," J. Biol. Dyn., vol. 14, no. 1, pp. 590-607, 2020, doi: 10.1080/17513758.2020.1788182.
[31] M. Rafiq, J. E. Macías-Díaz, A. Raza, and N. Ahmed, "Design of a nonlinear model for the propagation of COVID-19 and its efficient nonstandard computational implementation," Appl. Math. Comput., doi: https://doi.org/10.1016/j.apm.2020.08.082.
[32] R. Surendar, M. Muthtamilselvan, and R. Rakkiyappan, "LMI based sample data Controller for synchronization on the time delay Darcy-Brinkman model," J. Franklin Inst., doi: https://doi.org/10.1016/j.jfranklin.2022.06.020.
[33] S. Annas, M. Isbar Pratama, M. Rifandi, W. Sanusi, and S. Side, "Stability analysis and numerical simulation of SEIR model for pandemic COVID-19 spread in Indonesia," Chaos Solitons Fractals, vol. 139, 2020, p. 110072, doi: https://doi.org/10.1016/j.chaos.2020.110072.
[34] R. Ramesh and G. Arul Joseph, "SEIHR model for Indian COVID-19: trustworthiness of the government regulatory procedure for coronavirus aspects," Commun. Math. Biol. Neurosci., vol. 2024, Article ID 24, 2024, doi: https://doi.org/10.28919/cmbn/8407.